Consistent Surface Model for SPH-based Fluid Transport

Jens Orthmann[*]and Hendrik Hochstetter[†]and Julian Bader[‡]and Serkan Bayraktar[§]and Andreas Kolb[¶]
University of Siegen

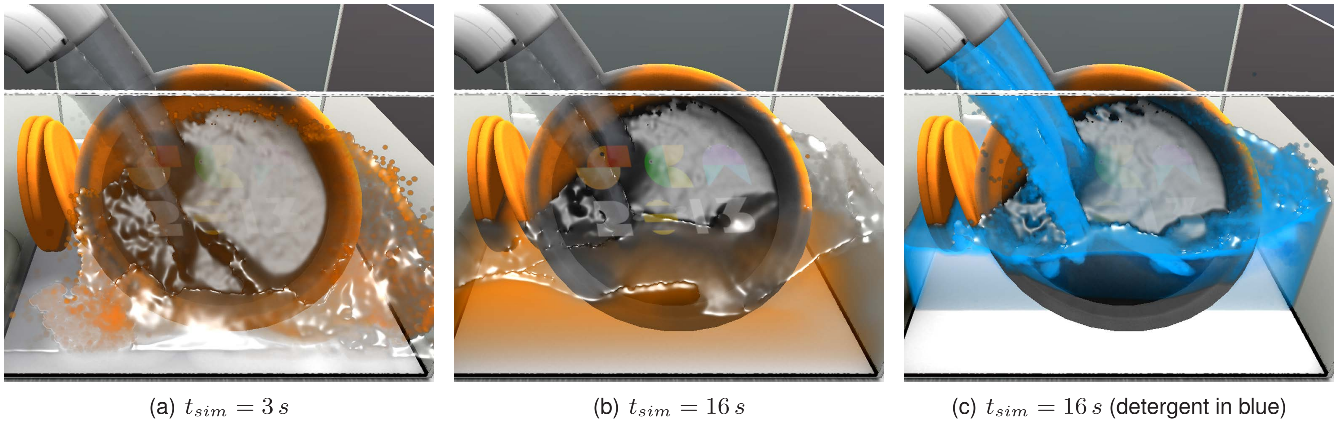
(a) $t_{sim} = 3\,s$ (b) $t_{sim} = 16\,s$ (c) $t_{sim} = 16\,s$ (detergent in blue)

Figure 1: *The pan's surface is cleansed from grease (orange) due to detergent concentration (blue in 1(c)) on the fluid's surface.*

Abstract

Surface effects play an essential role in fluid simulations. A vast number of dynamics including wetting of surfaces, cleansing, and foam dynamics are based on surface-surface and surface-bulk interactions, which in turn rely on a robust surface computation. In this paper we introduce a conservative Lagrangian formulation of surface effects based upon incompressible smoothed particle hydrodynamics (SPH). The key concept of our approach is to realize an implicit definition of the fluid's (free) surface by assigning each particle a value estimating its surface area. Based on this consistent surface representation, a conservative coupling of bulk and surface is achieved. We demonstrate the applicability and robustness of our approach for several types of surface-relevant effects including adsorption, diffusion and reaction kinetics.

CR Categories: I.3.5 [Computer Graphics]: Computational Geometry and Object Modeling—Physically based modeling I.3.7 [Computer Graphics]: Three-Dimensional Graphics and Realism—Animation

Keywords: SPH, surface reconstruction, effects, fluid simulation, reaction kinetics

1 Introduction

Since its introduction by Gingold, Monaghan [1977] and Lucy [1977], Lagrangian fluid simulation using smoothed particle hydrodynamics (SPH) is a well established method. Major advantages of this approach are mass conservation and the simple handling of free surfaces. There is a vast SPH literature dealing with fluid surfaces and interfaces and surface-related effects, e.g. to realize erosion [Kristof et al. 2009], density contrasts [Solenthaler and Pajarola 2008], diffuse materials [Losasso et al. 2008], porous flow [Lenaerts et al. 2008], and dynamics of foam [Ihmsen et al. 2012], only to name a few.

The reconstruction of surfaces and interfaces is the core component of any physically-based, surface-related effect simulation. There are two major options to solve this task in Lagrangian simulations, i.e. integrated particle-based approaches like color-fields [Adami et al. 2010] and separate, mainly mesh-based surface representations as presented by Yu et al. [2012] and Clausen et al. [2013]. However, integrated particle-based methods currently do not support free-surfaces, whereas explicit mesh-based techniques require complicated projections [Bertalmio et al. 2001; Adami et al. 2010] and frequent re-meshing operations to handle topology changes which makes it hard to capture singularities, especially in combination with a versatile rigid-fluid coupling (cf. [Akinci et al. 2012b]). While (hybrid) grid-based approaches such as FLIP [Ando et al. 2012] or PLS [Losasso et al. 2008] are able to preserve thin fluid sheets, they require a re-sampling between particle and grid, thus leading to numerical diffusion of quantity fields.

Our main goal is to provide a robust and consistent surface model which allows for a physically-based fluid simulation of reaction-diffusion processes. A mandatory step is to incorporate a conservative fluid transport of reactive quantities along surfaces and between surface and bulk, which for example allows us to simulate complex dynamics of detergents as shown in Fig.1. Like other surface active agents, so-called surfactants, detergents often get attracted to the surface, rather than remaining in the bulk. Combining this surface transport with reaction kinetics enables wash-out (cleansing) and coating of rigid objects as well as concentration controlled surface

[*] e-mail:jens.orthmann@uni-siegen.de
[†] e-mail:hochstetter@nt.uni-siegen.de
[‡] e-mail:bader@eti.uni-siegen.de
[§] e-mail:bayraktar@fb12.uni-siegen.de
[¶] e-mail:andreas.kolb@uni-siegen.de

SCA 2013, July 19 – 21, 2013, Anaheim, California.

effects like tension, wetting and dragging.

To the best of our knowledge, we are the first to present a consistent surface model in SPH in conjunction with conservative transport mechanisms within the fluid's surface and between surface and fluid volume (bulk), as well as surface-related reaction kinetics for SPH-based fluid simulations as discussed in Sec. 2. The **technical contributions** of this paper can be summarized as follows:

- In Sec. 4 we propose a novel and robust computation of surface area which correctly handles thin fluid sheets and other singularities frequent to free surface models (cf. Sec. 3) and which enables
- a conservative and SPH-consistent mechanism (two-way-coupling) for quantity transport within the surface and between surface and bulk (Sec. 5), and based on the coupling,
- a straightforward formulation of surface effects, including adsorption, diffusion and reaction kinetics (Sec. 6).

All our methods are incorporated into a fully data-parallel simulation framework as described in Sec. 7, the robustness and validity of which is demonstrated in Sec. 8. Sec. 9 then draws some final conclusions.

2 Related Work

SPH has been heavily used for simulation of fluids and we refer the reader to the surveys of Monaghan [2005] and Koumoutsakos et al. [2008] for a general overview.

Incompressibility is enforced by projection onto a divergence-free space [Cummins and Rudman 1999; Raveendran et al. 2011], a stiff equation of state [Becker and Teschner 2007] or by incorporating prediction-correction [Solenthaler and Pajarola 2009]. To enable large density contrasts [Solenthaler and Pajarola 2008] or versatile rigid-fluid couplings [Akinci et al. 2012b] it is preferable to replace the physical density [Müller et al. 2003] by a particle number density [Hu and Adams 2006]. Beside mass convection, a diffusive flux is incorporated to simulate thermodynamics [Müller et al. 2005] and transport of sediments [Kristof et al. 2009] or soluble substances [Cleary and Monaghan 1999]. Compact smoothing kernels [Müller et al. 2003], an adaptive sampling [Adams et al. 2007; Solenthaler and Gross 2011; Orthmann and Kolb 2012], adaptive time-steps [Ihmsen et al. 2010] and parallelization [Kolb and Cuntz 2005; Goswami et al. 2010; Ihmsen et al. 2011b] are essential in order to reduce simulation times. A rigid-fluid coupling is simulated using distance fields [Harada et al. 2007], via direct forcing [Becker et al. 2009], or by considering relative contributions of inhomogeneously sampled rigid particles [Akinci et al. 2012b].

Beside explicit surface models [Yu et al. 2012], which require complicated projections and re-meshing operations an implicit definition based on color gradient methods [Müller et al. 2003; Keiser et al. 2006; Akinci et al. 2012a] requires a second phase for stable simulation [Solenthaler and Pajarola 2008; Adami et al. 2010], which cannot be adaptively sampled by ghost particles [Schechter and Bridson 2012] as gradients are sensitive to irregular particle structures [Becker and Teschner 2007]. Signed distance functions are employed [Solenthaler et al. 2007b; Adams et al. 2007] to reconstruct smooth surfaces [Zhu and Bridson 2005; Solenthaler et al. 2007a; Onderik et al. 2011] and enable computation of anisotropy information [Yu and Turk 2010] aiming for surface reconstruction or capturing [Hieber and Koumoutsakos 2005].

SPH has been used in a variety of surface effects, ranging from temperature modulated viscosity [Stora et al. 1999], melting and solidification [Solenthaler et al. 2007a], changing solid conditions of ice [Iwasaki et al. 2010], simulations of trapped air [Müller et al. 2005], bubbles [Hong et al. 2008; Ihmsen et al. 2011a] and diffuse materials [Losasso et al. 2008; Ihmsen et al. 2012], wetting effects for granular materials [Rungjiratananon et al. 2008; Lenaerts and Dutré 2009] and physically-based erosion of terrains [Kristof et al. 2009]. However, none of these methods simulates a fluid transport on surfaces. In computational physics, Adami et al. [2010] presented an approach for surfactant dynamics not applicable to free-surface scenarios (see also Sec. 8). In contrast, we utilize an implicit signed distance, which leads to consistent bulk and surface representation supporting free surfaces as well as phase interfaces.

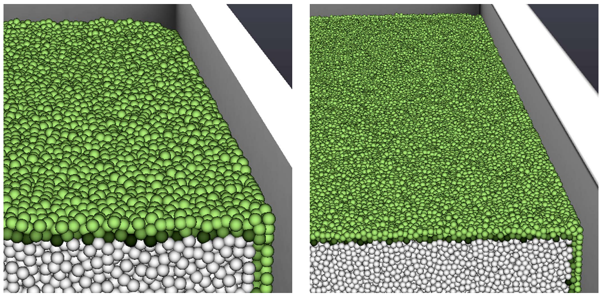

Figure 2: *A discretization of the surface delta function Eq.* (4) *results in a narrow band of surface particles (green) which thickness depends on the particle resolution (doubled from left to right).*

3 SPH Background

In SPH, a quantity field S is reconstructed over all particles j in the local neighbourhood of sampling position **x** [Gingold and Monaghan 1977]:

$$S(\mathbf{x}) = \sum_j S_j\, V_j\, W_j(\mathbf{x}) \tag{1}$$

where $W_j(\mathbf{x}) = W(r,h) = W(||\mathbf{x} - \mathbf{x}_j||, h)$ (or W_{ij} if $S_i = S(\mathbf{x}_i)$) is a radially symmetric smoothing kernel [Müller et al. 2003] with compact support h and V_i is a particle's dynamic volume. The assumption of constant rest density ρ_0 [Solenthaler and Pajarola 2008] leads to a particle number density $n_i = \sum_j v_j\, W_{ij}$, where v_i is a particle's rest volume. As a result, $V_i = \frac{m_i}{\rho_i} = \frac{\rho_0\, v_i}{\rho_0\, n_i} = \frac{v_i}{n_i}$, which for incompressible fluids yields $V_i \approx v_i$ in the bulk, since here $n_i \approx 1$. To correct the neighbour deficiency close to free surfaces we enforce $n_i \geq 1$.

In general, the free fluid-air interface $\partial\Omega := \{\mathbf{x} \,|\, \phi(\mathbf{x}) = 0\}$ is defined as the zero iso-contour of the following signed distance function [Zhu and Bridson 2005]:

$$\phi(\mathbf{x}) = ||\mathbf{x} - \mathbf{m}(\mathbf{x})|| - d, \tag{2}$$

where d is the desired distance between surface and particles, which in our simulation equals the particle's radius, and $\mathbf{m}(\mathbf{x})$ is the center of the local iso-density distribution [Onderik et al. 2011]:

$$\mathbf{m}(\mathbf{x}) = \frac{\sum_j \mathbf{x}_j\, V_j\, W_j(\mathbf{x})}{\sum_j V_j\, W_j(\mathbf{x})}. \tag{3}$$

Still, one needs a robust model of the singularity at the surface in order to simulate quantity transport and reactions on the surface.

4 Computation of Surface Area

To compute stable surface fields we need a robust and reliable estimation of surface area. According to Bertalmio et al. [2001],

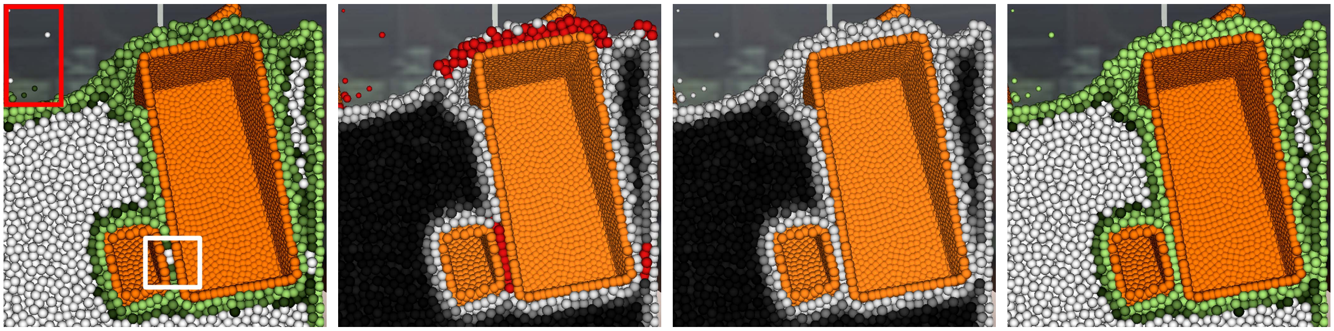

(a) Erroneous a_i (b) Singularity (c) Corrected δ_i (d) Corrected a_i

Figure 3: *Singularities, e.g. as induced by rigid objects (orange), result in erroneous areas a_i (highlighted in 3(a)). A detection of singular regions (red in 3(b)) enables a correction of delta values δ_i (increasing from black to grey in 3(c)), which leads to robust areas a_i (cf. 3(d)).*

it is advantageous to represent such a lower dimensional surface as the level-set of a higher dimensional function, thus avoiding re-meshing or error-prone computations on triangulated surfaces. Hence, the area of the fluid's surface is defined by integrating a surface delta function over the fluid volume Ω, i.e. $\int_\Omega \delta_I(\mathbf{x})\,\partial\mathbf{x}$ (cf. Osher and Fedkiw [2002]).

Our idea is to sample the iso-contour as defined in the last section with bulk particles as shown in Fig. 2. Due to the resulting consistent SPH-based representation of bulk and surface, the delta function is then reconstructed by the following integral interpolant over the local particle neighbourhood:

$$\delta_I(\mathbf{x}) = \int_\Omega \hat{\delta}(\mathbf{x}_j)\, W_j(\mathbf{x})\, \partial\mathbf{x}_j, \tag{4}$$

where $\hat{\delta}(\mathbf{x}_j) = \delta(\phi(\mathbf{x}_j))\,||\nabla\phi(\mathbf{x}_j)||$. By assuming that particles locally approximate a flat surface, we are able to approximate the three-variate delta function depending on the sampling position by a one-variate function depending only on the distance to the surface, i.e. $\hat{\delta}(\mathbf{x}_j) \approx \delta(\phi(\mathbf{x}_j))$ (see App. A). Note that this is a valid approximation, since due to the SPH-based distance function, surface resolution is directly linked to the particle resolution. Thus, surface structures can only emerge up to the size of a particle's support radius as also discussed later in Sec. 8. Consequently, a particle's contribution to the surface simplifies to

$$\partial a_i \approx \partial\mathbf{x}_i \int_\Omega \delta(\phi(\mathbf{x}_j))\, W_{ij}\, \partial\mathbf{x}_j\ , \tag{5}$$

where $\partial\mathbf{x}_i$ is the differential volume of particle i. An integration of differential particle areas $\partial a_i = \partial\mathbf{x}_i\, \delta_I(\mathbf{x}_i)$ then yields the area of the fluid's surface.

In practice, as summarized in Fig. 4, the integral interpolant $\delta_I(\mathbf{x})$ is approximated by a summation interpolant $\delta_S(\mathbf{x})$ using discrete particle volumes (see Sec. 4.2) in combination with a smeared-out version of the delta function (see Sec. 4.1). As a result, the surface extends into the fluid's bulk and leads to a narrow band of contributing particles. Each particle within this band represents a fraction of surface area a_i, depending on its distance to the surface. However, unlike particle volumes v_i, a particle's fraction of surface area is not constant due to internal and external forces changing the surface topology. Thus, in order to stably handle thin fluid sheets we correct delta values in singular regions as described in Sec. 4.3.

4.1 Delta Function Approximation

Since due to discretization, the delta function would be zero almost everywhere, we smear out the iso-contour $\delta\Omega$ over the local fluid volume using an SPH-based smoothing kernel as shown in Fig. 4(a). However, in combination with small support radii, the distance function may return slightly fluctuating distance values ϕ_i over time, since the computation of the local mass center is prone to changing particle neighbourhoods. Thus, in practice it is better to approximate the surface delta function by the following half-sided linear tent-kernel:

$$\delta(\phi) = \frac{1}{d}\begin{cases} (1+\frac{\phi}{d}) & \text{if } \phi < 0 \\ 0 & \text{otherwise,} \end{cases} \tag{6}$$

which only depends on the distance to the iso-contour at $\phi(\mathbf{x}) = 0$ for which by definition $\phi(\mathbf{x}) \geq -d$ holds. During simulation we integrate discrete values $\delta_i = \delta(\phi(\mathbf{x}_i))$ evaluated at particle locations $\mathbf{x}_i \in \Omega-$ in order to compute a surface area. Due to the normalization property, i.e. $\int_{-d}^{d} \delta(\phi)\,\partial\phi = 1$, the surface area is then linearly distributed over fluid particles and the smoothing of the area is directly related to the size of d.

4.2 Interpolation of Particle Areas

In order to determine how much of the surface area is represented by a particle, we have to integrate the surface delta function as derived in the last section over a particle's support h (see Fig. 4(b)). In detail, the corresponding SPH approximation for Eq. (5) yields

$$a_i = V_i\, \delta_S(\mathbf{x}_i) = V_i \sum_j \delta_j\, V_j\, \hat{W}_{ij}. \tag{7}$$

However, the surface $\partial\Omega$ is only sampled for particles in the fluid domain $\Omega-$. We therefore have to correct the resulting volume

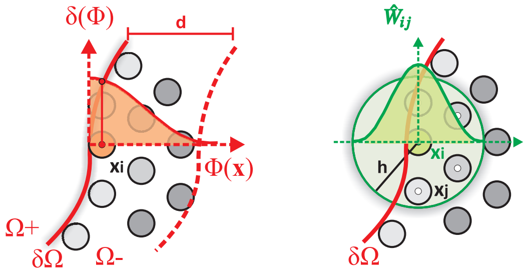

(a) Delta Function (b) Corrected Interpolation

Figure 4: *Interpolation of particle areas using a corrected SPH reconstruction of a half-sided smeared-out delta function.*

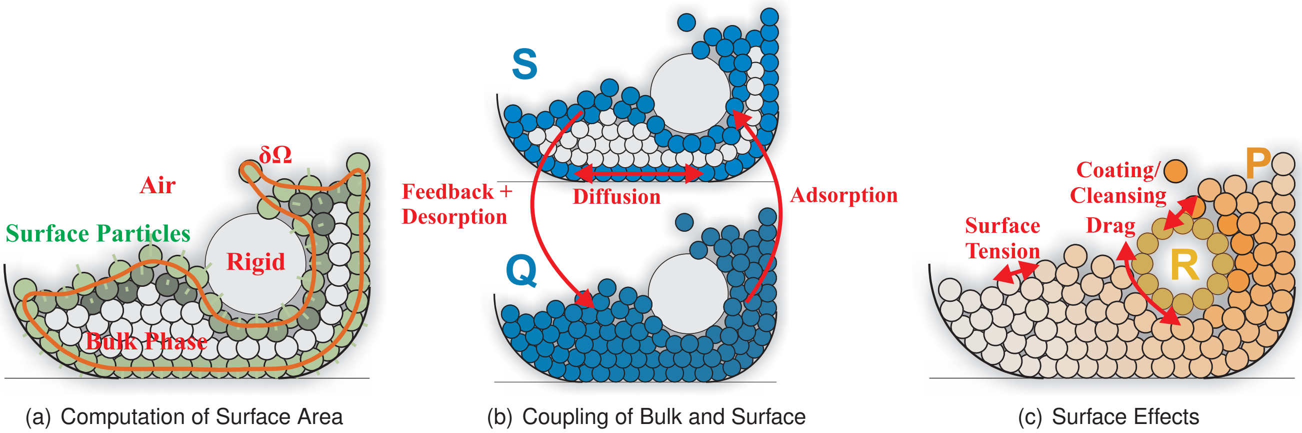

(a) Computation of Surface Area

(b) Coupling of Bulk and Surface

(c) Surface Effects

Figure 5: *Simulation overview: first particles sample the implicitly defined surface $\delta\Omega$ (cf. 5(a)). Surface particles (green) then constitute a quantity field S on the surface, and together with bulk particles (white), a quantity field Q in a fluid's bulk (cf. 5(b)). Dependening on the application, S reduces surface tension and fluid drag or reacts with substances R (yellow) on rigid surfaces to products P (orange) (cf. 5(c)).*

deficiency due to the under-resolved particle neighbourhood in $\Omega+$. Thus we use the following adapted weighting kernel [Bonet and Kulasegaram 2002]

$$\hat{W}_{ij} = \frac{W_{ij}}{\sum_l V_l W_{il}},$$

which leads to an consistent interpolation of constant functions at fluid boundaries. As a result of the interpolation, particles close to the surface have a high contribution. The closer a particle, the more it contributes to the surface. Due to the definition of the distance function, a disturbance of regular particle structures, as caused by the flow-field, leads to small area values in the fluid bulk. Thus, we consider a particle not to be part of the surface as long as its area is below or equal $a_{\min}$. However, values δ_i need to be corrected in highly under-resolved regions as described in the next section.

4.3 Stable Handling of Thin Fluid Sheets

During simulation regular but deficient particle neighbourhoods can emerge which might lead to erroneous area values as shown in Fig. 3(a). Singular cases might be identified by setting a lower threshold for the number of neighbouring particles, but dense and strongly anisotropically distributions still would remain unidentified. A better description for local particle distributions is the weighted covariance matrix of a particle i, given as [Yu and Turk 2010]

$$\mathbf{C}_i = \frac{\sum_j (\mathbf{x}_j - \mathbf{m}_i)(\mathbf{x}_j - \mathbf{m}_i)^T W_{ij}}{\sum_j W_{ij}} \in \mathbb{R}^{3x3}. \tag{8}$$

Since we want to detect singular particle structures, the determinant of a particle's covariance matrix naturally reveals flat or planar particle neighbourhoods. Accordingly, if $|\mathbf{C}_i| < \epsilon_c$ or if a particle i has less than 30 neighbours (red particles in Fig. 3(b)) we will set $\delta_i = \delta_{\max}$ (assuming a flat surface) leading to a corrected approximation of delta values as shown in Fig. 3(c). Similarly, since rigid particles k are directly sampled on the explicit rigid surfaces, we pre-compute area values a_k of rigid particles by assuming $\delta_k = \delta_{\max}$.

The simulation requires time-coherent area values in order to avoid fluctuation of quantity fields. However, thin fluid structures may be under rapid progress. Due to the temporal coherence of particle systems, we also apply a temporal smoothing of particle areas in singular regions, which is computed as

$$\delta_i(t+1) = (1-\kappa)\delta_i(t) + \kappa\delta_i(t+1)^*, \tag{9}$$

where $\delta_i(t+1)^*$ is the approximated surface delta function according to Eq. (6) and where κ defines the rate of adjustment to new values $\delta_i(t+1)^*$. In our examples we set $\kappa \in [0.1, 0.5]$ for thin sheets and $\kappa = 1$ for all other regions.

5 Integrated Surface Model

The strength of our surface area computation is that quantity fields on a surface can now be reconstructed over the fluid volume by using Eq. (1) leading to a consistent representation of bulk and surface. The underlying Lagrangian SPH simulation then acts as a "particle-pool" for quantity fields defined on surfaces, as shown in Fig. 5. Particles are divided into two groups: *surface particles* (green) within a small layer around the surface, i.e. where $a_i > a_{\min}$, and *bulk particles* (white). Surface particles have a double role during simulation: Like bulk particles, they contribute to a quantity field Q and at the same time, they constitute a quantity field S on the surface which is then responsible for surface effects.

Even if our method is not restricted to scalar quantities, we consider Q_i and S_i as concentrations of a substance defined with respect to a particle's volume or area. Depending on the transport properties of quantities, particles may have an attribute $\overline{S}_i = a_i S$ representing molar mass adhered to a particle's surface and an attribute $\overline{Q}_i = Q_i v_i$ representing the mass transported in bulk. Substances require both attributes if they exhibit different behaviour for surface and bulk (cf. Fig. 6). Total mass of such anisotropic distributed substances is $\sum_i \overline{Q}_i + \overline{S}_i$. If formulation of transport in bulk and on surface are equal, only a single attribute representing the total number of molecules in bulk $\overline{Q}_i$ is required (cf. Fig. 7). Naturally, for isotropically distributed substances the concentration per area is proportional to the concentration per volume, i.e. $S_i = \frac{v_i}{a_i} Q_i$.

A change of surface concentrations is defined with respect to particle areas:

$$\frac{\partial}{\partial t} S_i = \frac{1}{a_i} \sum_j \Gamma_{i \leftarrow j},$$

where $\Gamma_{i \leftarrow j}$ represents a mass flux from particle j to particle i, thus is defined with respect to absolute quantities, i.e. $\overline{S}_i$ and $\overline{Q}_i$. While mass is trivially conserved for a flux computed in bulk, a quantity flux from bulk to surface and on the surface require symmetric formulations, i.e. $\Gamma_{i\leftarrow j} = -\Gamma_{j\leftarrow i}$. In the following, we develop will the building blocks for a conservative transport between bulk and surface and on surfaces which we apply to surfactant dynamics and transport of paint in Sec. 6.

5.1 Coupling of Bulk and Surface

Dynamics of a fluid's bulk and surface are strongly interconnected. The bulk acts as a source and as a sink for the surface. Thus, mass is transferred between two different kinds of particles, surface particles i and bulk particles j (which might be one and the same particle, i.e. $i = j$). Consequently, a transport mechanism between bulk and surface is not symmetric per se. To ensure conservation, we compute a quantity flux with focus on surface particles i and assume the opposite flux for bulk particles j:

$$\frac{\partial}{\partial t} S_i = \frac{1}{a_i}\sum_j \Gamma_{i\leftarrow j}, \quad \text{and} \quad \frac{\partial}{\partial t} Q_j = \frac{1}{v_j}\sum_i -\Gamma_{i\leftarrow j}. \qquad (10)$$

That way we take as much of a quantity from bulk as the surface receives and vice versa.

5.2 Unified Free-Surfaces and Interface Dynamics

Due to non-constant particle areas, standard symmetrization techniques, i.e. gradient approximations [Colin et al. 2006] or integral approximations [Cleary and Monaghan 1999], do not lead to symmetric formulations of fluxes. Therefore, we enforce conservation explicitly by averaging pairwise contributions between surface particles, i.e. using $\Gamma_{i\leftarrow j} = -\Gamma_{j\leftarrow i}$:

$$\frac{\partial}{\partial t} S_i = \frac{1}{a_i}\sum_j \Gamma_{i\leftarrow j} = \frac{1}{a_i}\sum_j \frac{1}{2}[\Gamma_{i\leftarrow j} - \Gamma_{j\leftarrow i}], \qquad (11)$$

where i and j might also be part of different phases. In contrast to the averaging of particle attributes as proposed by Müller et al. [Müller et al. 2003] we use Newton's action = reaction principle. Please note that for adjacent phases iso-contours do in general not match exactly. However, pairwise averaging of contributions naturally corrects such discontinuities.

6 Application to Fluid Transport

In this section we apply our surface model to specific fluid transport phenomena. Our surface model is especially well suited to simulate dynamics of detergents as shown in Fig. 1. Detergents as other surfactants show very complex behaviour on fluid surfaces, including adsorption at surfaces (see Sec. 6.1) and strong surface diffusion (see Sec.6.2). We also apply our integrated surfaces to simulate paint (cf. Fig. 7) which is transported by convection only. Beside transport, we model chemical reactions, in detail coating (see Sec.6.4) and cleansing (see Sec.6.3). Additionally, a surface concentration alters surface tension as proposed by Becker and Teschner [2007] and fluid drag similar to Akinci et al. [2012b] as shown in Fig.10.

6.1 Adsorption

The driving mechanism for simulation of detergents and other surfactants is the well known Langmuir-Hinshelwood mechanism [Berthier and Silberzan 2009] which describes how much of a so-called "free" substrate or target $\overline{Q}_j$ in a carrier fluid is adsorbed on a surface. Fig. 6 shows the importance of adsorption for a falling drop of detergent. The net rate of adsorbed substrates at surface particle i mainly depends on the presence of targets at neighbouring bulk particles j, which by applying Eq. (10) is computed as

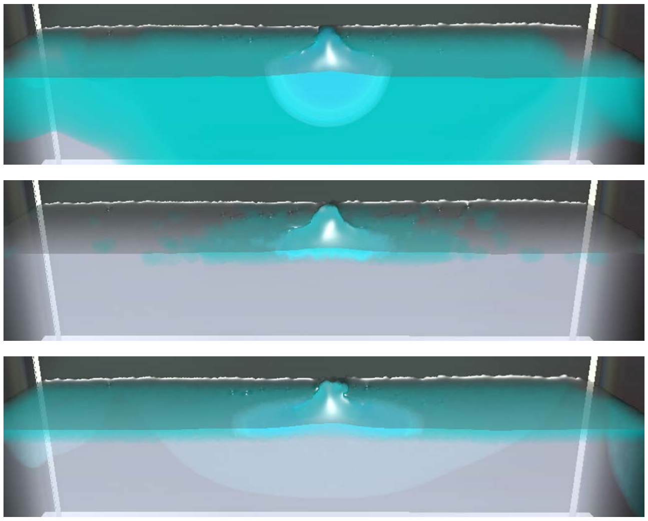

Figure 6: *Falling drop of detergent. From top to bottom: no adsorption $\sigma_a = 0$ leads to diffusion into the bulk, while $\sigma_a > 0 \wedge \sigma_d = 0$ leads to a local concentration on the surface. $\sigma_a > 0 \wedge \sigma_d > 0$ results in homogeneous concentration on the surface.*

$$\Gamma^a_{i\leftarrow j} = \left[\sigma_a \overline{Q}_j \left(\overline{S}_0 - \overline{S}_i\right) \; - \; \sigma_f \overline{S}_i\right] V_j W_{ij},$$

where σ_a defines the speed of adsorption and where the total number of available capture sites $\overline{S}_0$ limits the adsorption process. Over time, adsorbed targets constantly dissociate from the surface as controlled by σ_f. Particles which are drawn under the surface, transfer mass back to nearby bulk particles by setting $\sigma_f > 0$ and $\sigma_a = 0$.

6.2 Diffusion

Since S is non-zero only at the surface, we can approximate a surface diffusion as shown in Fig. 6 by averaging (cf. Eq. (11)) the integral approximation as proposed by Cleary et al. [1999]:

$$\Gamma^d_{i\leftarrow j} = \sigma_d \left(S_i - S_j\right) \left(a_i V_i + a_j V_j\right) \frac{\partial}{\partial r} W_{ij},$$

where σ_d is an isotropic diffusion constant. Note that i, j are restricted to surface particles in order to avoid diffusion into the bulk.

6.3 Cleansing

With detergent concentration adhered to the surface we are able to simulate a cleansing [Rosen and Kunjappu 2004] of rigid surfaces as shown in Fig. 1 and 10. Detergent molecules $\overline{S}$ solve and enclose grease molecules on rigid surfaces $\overline{R}$ thereby forming products or micelles $\overline{P}$ which dissolve into the bulk. The speed of this bi-molecular reaction is then defined via a simple rate law which linearly depends on the rate constant σ_r and the total number of molecules of both reactants, i.e. $\sigma_r \overline{S}\,\overline{R}$, which in SPH reads

$$\Gamma^r_{i\leftarrow k} = \sigma_r \overline{S}_i \overline{R}_k \, \frac{1}{2}(V_i + V_k)\, W_{ij}.$$

By coupling of bulk and surface, the reaction rate is then defined as

$$v_i \frac{\partial}{\partial t} P_i = -a_i \frac{\partial}{\partial t} S_i = -a_k \frac{\partial}{\partial t} R_k = \sum_k \Gamma^r_{i\leftarrow k},$$

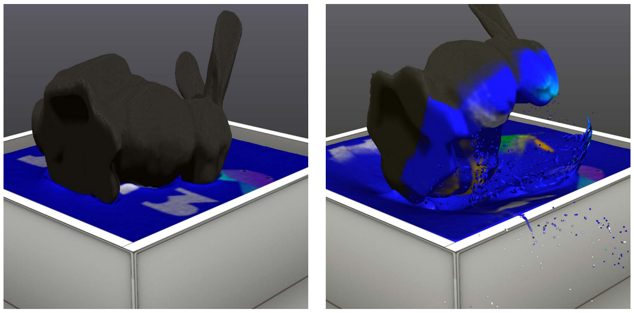

Figure 7: *Coating of a Stanford Bunny.*

where i are fluid particles and k are rigid particles. Note that we have used both Eq. (10) and Eq. (11) to decribe a conservative reaction.

6.4 Coating

A coating of rigid objects as shown in Fig. 7 is modelled as a unimolecular reaction where one molecule of paint on the fluid's surface $\overline{S}$ is transformed into one molecule of paint sticking to rigid surfaces $\overline{R}$. The coating process depends on the total number of molecules $\overline{S}$ close to the rigid object's surface, for which the reaction reads:

$$\Gamma^r_{i\leftarrow k} = -\sigma_r \overline{S}_i \, \frac{1}{2}(V_i + V_k)\, W_{ij},$$

where σ_r is a rate constant defining the reaction speed. Molecular mass of both substances then changes by

$$v_j \, \frac{\partial}{\partial t} Q_j = -a_k \, \frac{\partial}{\partial t} R_k = \sum_k \Gamma^r_{i\leftarrow k},$$

where Eq. (10) has been used. We stop a deposition of material when rigid particles reach a maximum concentration of $R_{\max} = 1$.

7 Implementation Details

In all examples we have employed an incompressible convection [Solenthaler and Pajarola 2009] coupled with rigid objects [Akinci et al. 2012b] in combination with matter diffusion [Monaghan 2005] and an adaptive time-stepping mechanism [Ihmsen et al. 2010]. Note that any other incompressible SPH solver can be used for the bulk dynamics. While we use a second order leapfrog integration for convection, we integrate a diffusive flux using an explicit Euler integration which is sufficient as long as diffusion takes place at much smaller scale than convection.

For field reconstruction we have set $h = 2d$, which results in a rest distance of $0.92h$ between particles and around 30 neighbours per particle in combination with smoothing kernels as proposed by Müller et al. [2003]. For the computation of distance values and anisotropy we have increased the smoothing radius to $2.5h$ to obtain reliable results. To speed up simulation, we recompute $\delta_i(t+1)*$ only every 10-th frame in regions of small divergence, i.e. where $\nabla \cdot \mathbf{u}_i < \epsilon_u$, since in these regions $\frac{\partial}{\partial t}\delta_i = 0$ (see App. B). Note that all constants necessary to compute a surface area (cf. Sec. 4.3), are precomputed from pre-defined incompressible particle configurations as shown in Fig. 8. For more details on the simulation, we refer to the accompanying 2D Matlab®implementation.

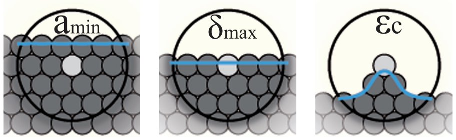

Figure 8: *Area constants are pre-computed for reference particles (white) within user-defined particle configurations.*

Scene	"Pan"	"Flooding"	"Drop"	"Kinect®"	"Bunny"
σ_r/σ_d	10/10	70/10	−/10	40/10	40/−
σ_a/σ_f	10/0.1	10/0.1	10/0.0	10/0.1	−/−
Snapshot t_{sim}	23 sec.	30 sec	3 sec	20 sec	11 sec
Avg.δt [ms]	2	1.5	2	1.5	2
# fluid ptcls	2.1M	1.1M	1.1M	0.75M	4.7M
# surface ptcls	350k	200k	141k	300k	506k
Delta Func. [ms]	35.9	30.2	28.3	60.0	65.4
Surface Area [ms]	14.0	14.8	11.5	9.2	61.5
Adsorption [ms]	22.1	19.0	12.2	14.9	26.7
Diffusion [ms]	3.4	2.8	1.5	3.6	33.2
Reactions [ms]	15.3	17.5	0	12.0	0.65
Time per Frame	**312**	**261**	**203**	**252**	**693**

Table 1: *GPU per frame timings (in msec) for presented scenes.*

8 Results and Discussion

We have tested our method in various scenarios in order to show its versatility, including a washing of dishes (Fig. 1), the flooding of a valley (Fig. 10), a complex Kinect®scene (Fig. 12), coating of a rigid surface and the evolution of a single drop of detergent (Fig. 6). All results were obtained on an Intel Dual-Core 3.3 GHz with an NVidia GTX 580 with 1.5 GB VRAM. Simulation achieves interactive frame-rates even for a few million particles as shown in Tab. 1 and it is expected that computation cost will linearly scale for higher particle counts. For visualization of concentrations we have utilized an SPH-based volume rendering approach [Orthmann et al. 2010] in combination with an image-based [van der Laan et al. 2009] or marching cubes based [Akinci et al. 2012a] surface rendering. Please note, that the aim of the renderings is not to produce photo-realistic images but to visualize the underlying dynamics for which we also refer to the accompanying video.

Fig. 9 compares our surface area to the color gradient based interfaces used by Adami et al. [2010] (note, that we apply $2.5h$ sampling radius in contrast to the proposed $6h$, which would lead to even thicker surface layers). Most importantly, our method supports free surfaces and avoids error-prone normal projection for surface dynamics; we do not require any normal computation. Due to the robust formulation, even complex scenes with highly irregular point distribution, e.g. as originating from a Kinect®sensor (cf. Fig. 12), are stably handled without reducing integration time-step. Furthermore, our integrated surface model is able to conserve mass within

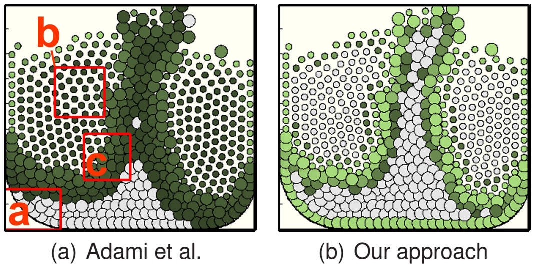

(a) Adami et al.

(b) Our approach

Figure 9: *Comparison to interface approximation of Adami et al. : Our approach handles free-surface (a), irregular particle structures (b), and yields thin interfaces (c).*

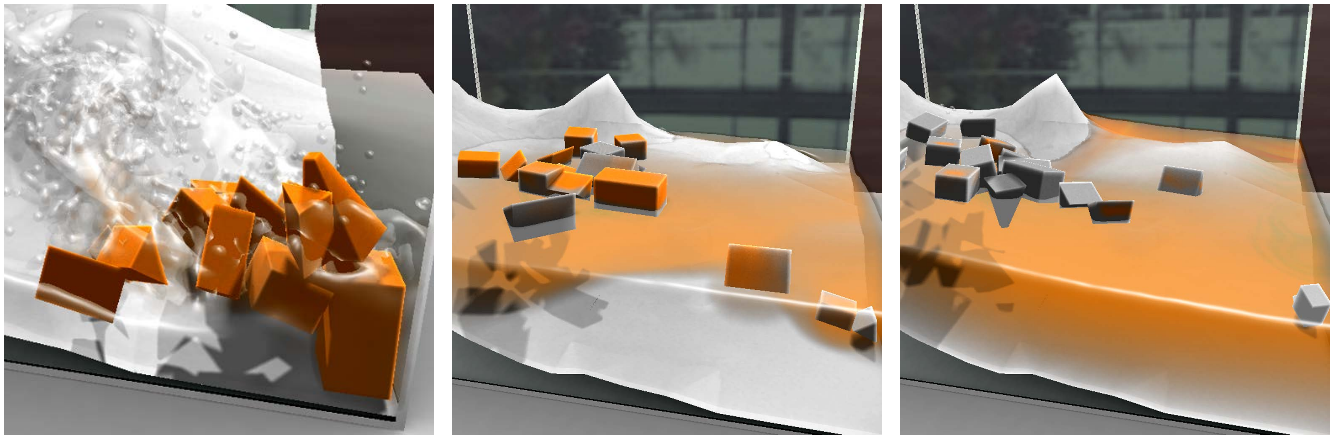

(a) $t_{sim} = 6\,s$ (b) $t_{sim} = 30\,s$, $Q_{init} = 0.1$ (c) $t_{sim} = 30\,s$, $Q_{init} = 1.0$

Figure 10: *Flooding of a valley shown for two time-steps. Emitting less detergent concentration not only results in less cleansing but also results in a different outcome of the convection due to stronger surface tension and fluid drag (cf. 10(b) and 10(c)).*

highly turbulent free-surface flows and for complex rigid-fluid interactions as shown in Fig. 10.

The main limitation of our current implementation is that the surface resolution is directly linked to the bulk resolution, since we use uniform particle sizes. As can be seen in Fig. 2, the particle resolution directly relates to the thickness of the surface and influences its appearance and the transport dynamics (cf. Fig. 6). Due to the underlying implicit distance function (cf. Eq. (2)), particles can only capture details equal to the particle resolution. In Fig. 11 we have sampled an analytically defined signed-distance function to illustrate this relation. The higher the particle resolution the more complex surface structures can emerge and the more accurately surface details can be captured. Beside visual appearance, the accuracy of the approximation also depends on the particle resolution. Note, with increasing resolution, the surface area converges towards the ground truth area of the underlying sine function. However, we believe that in the future the surface resolution can be easily decoupled from the bulk resolution by incorporating an adaptive particle sampling as proposed by Orthmann and Kolb [2012] or Solenthaler and Gross [2011]. Moreover, the effect simulation would benefit from more complex reaction kinetics, which account for temperature dependencies or non-linear reactions like explosions and can easily be enriched with other effects like foam dynamics.

9 Conclusion

We have presented a novel approach for robust computation of a fluid's (free) surface, which is the core concept for any physically-based simulation of surface transport. Therefore, we have introduced a consistent formulation for a fluid's surface and bulk along with a conservative coupling between both fields. Based on this formulation, we have realized a transport model which incorporates a separate diffusion for surface and bulk, as well as a model for reactions at fluid-rigid interfaces. We have evaluated our approach using various application scenarios. Due to its robustness it seems promising that our consistent surface model has a high potential to improve related research areas such as surface reconstruction.

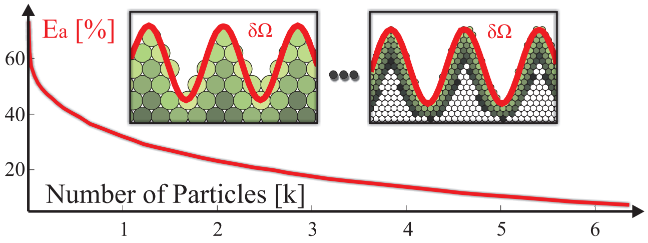

Figure 11: *Approximation error E_a. With increasing resolution, the surface area converges towards the ground truth area $\delta\Omega$ and particles are able to reconstruct surface structures more accurately.*

Acknowledgements

We would like to express our gratitude to Willi Gräfrath for his patience in the audio recording and for speaking the text in the video and Maik Keller for providing the Kinect® data. We also wish to thank the anonymous reviewers for their valuable comments and suggestions which greatly helped to improve the quality of the paper.

References

ADAMI, S., HU, X. Y., AND ADAMS, N. A. 2010. A conservative SPH method for surfactant dynamics. *J. Comput. Phys. 229*, 5, 1909–1926.

ADAMS, B., PAULY, M., KEISER, R., AND GUIBAS, L. J. 2007. Adaptively sampled particle fluids. *ACM Trans. Graph. 26*, 48:1–48:7.

AKINCI, G., IHMSEN, M., AKINCI, N., AND TESCHNER, M. 2012. Parallel surface reconstruction for particle-based fluids. *Computer Graphics Forum 31*, 1797–1809.

AKINCI, N., IHMSEN, M., AKINCI, G., SOLENTHALER, B., AND TESCHNER, M. 2012. Versatile rigid-fluid coupling for incompressible SPH. *ACM Trans. Graph.*, 62:1–62:8.

ANDO, R., THÜREY, N., AND TSURUNO, R. 2012. Preserving fluid sheets with adaptively sampled anisotropic particles. *IEEE Transactions on Visualization and Computer Graphics 18*, 8, 1202–1214.

BECKER, M., AND TESCHNER, M. 2007. Weakly compressible SPH for free surface flows. In *Proc. Symp. Comp. Anim.*, 209–217.

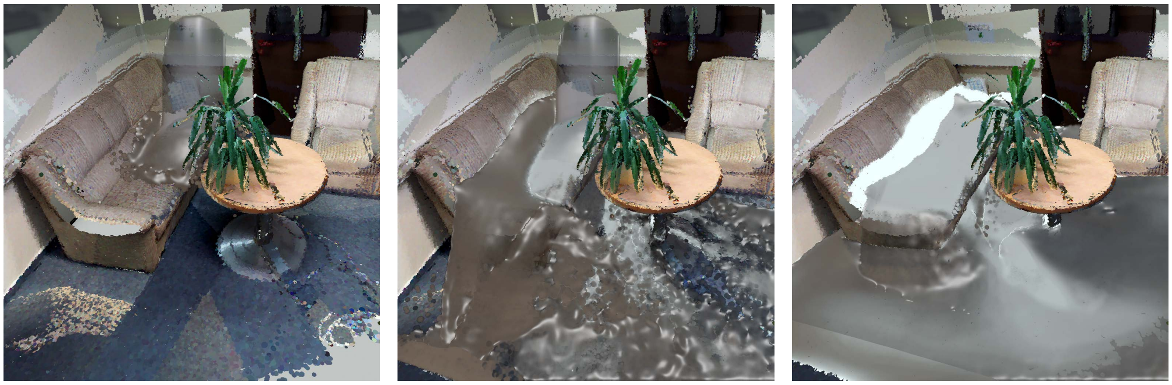

Figure 12: *Complex room-scene acquired with a Kinect® camera. Multiple material colors are washed out over time resulting in dirty water.*

Becker, M., Tessendorf, H., and Teschner, M. 2009. Direct forcing for lagrangian rigid-fluid coupling. *IEEE Trans. Vis. & Comp. Graph. 15*, 3, 493–503.

Bertalmio, M., Cheng, L.-T., Osher, S., and Sapiro, G. 2001. Variational problems and partial differential equations on implicit surfaces: The framework and examples in image processing and pattern formation. *J. Comput. Phys. 174*, 759–780.

Berthier, J., and Silberzan, P. 2009. *Microfluidics for biotechnology*. Artech House integrated microsystems series. Artech House.

Bonet, J., and Kulasegaram, S. 2002. A simplified approach to enhance the performance of smooth particle hydrodynamics methods. *J. Applied Mathematics & Computation 126*, 2-3, 133–155.

Clausen, P., Wicke, M., Shewchuk, J., and O'Brien, J. 2013. Simulating liquids and solid-liquid interactions with lagrangian meshes. *ACM Trans. Graph. 32*, to appear.

Cleary, P. W., and Monaghan, J. J. 1999. Conduction modelling using smoothed particle hydrodynamics. *J. Comput. Phys. 148*, 227–264.

Colin, F., Egli, R., and Lin, F. Y. 2006. Computing a null divergence velocity field using smoothed particle hydrodynamics. *J. Comput. Phys. 217*, 2, 680–692.

Cummins, S. J., and Rudman, M. 1999. An sph projection method. *J. Comput. Phys. 152*, 2 (July), 584–607.

Gingold, R., and Monaghan, J. 1977. Smoothed particle hydrodynamics: theory and application to non-spherical stars. *Notices of the Royal Astronomical Society 181*, 375–389.

Goswami, P., Schlegel, P., Solenthaler, B., and Pajarola, R. 2010. Interactive SPH simulation and rendering on the GPU. In *Proc. Symp. Comp. Anim.*, 55–64.

Harada, T., Koshizuka, S., and Kawaguchi, Y. 2007. Smoothed particle hydrodynamics on GPUs. *Proc. Computer Graphics International*, 63–70.

Hieber, S. E., and Koumoutsakos, P. 2005. A lagrangian particle level set method. *J. Comput. Phys. 210*, 342–367.

Hong, J.-M., Lee, H.-Y., Yoon, J.-C., and Kim, C.-H. 2008. Bubbles alive. *ACM Trans. Graph. 27*, 3, 48:1–48:4.

Hu, X. Y., and Adams, N. A. 2006. A multi-phase SPH method for macroscopic and mesoscopic flows. *J. Comput. Phys. 213*, 2, 844–861.

Ihmsen, M., Akinci, N., Gissler, M., and Teschner, M. 2010. Boundary handling and adaptive time-stepping for PCISPH. In *Proc. Virt. Reality Interaction & Phys. Sim.*, 79–88.

Ihmsen, M., Bader, J., Akinci, G., and Teschner, M. 2011. Animation of air bubbles with SPH. In *Proc. Int. Conf. Comp. Graph. Theory & App. (GRAPP)*, 225–234.

Ihmsen, M., Akinci, N., Becker, M., and Teschner, M. 2011. A parallel SPH implementation on multi-core CPUs. *Computer Graphics Forum 30*, 99–112.

Ihmsen, M., Akinci, N., Akinci, G., and Teschner, M. 2012. Unified spray, foam and bubbles for particle-based fluids. *Vis. Comput. 28*, 669–677.

Iwasaki, K., Uchida, H., Y.Dobashi, and T. Nishita, " (PG 2010), t. a. 2010. Fast particle-based visual simulation of ice melting. *Computer Graphics Forum 29*, 7, 2215–2223.

Keiser, R., Adams, B., Guibas, L. J., Dutr, P., and Pauly, M. 2006. Multiresolution particle-based fluids. Tech. rep., ETH.

Kolb, A., and Cuntz, N. 2005. Dynamic particle coupling for GPU-based fluid simulation. In *Proc. Symp. Sim. Technique*, 722–727.

Koumoutsakos, P., Cottet, G.-H., and Rossinelli, D. 2008. Flow simulations using particles: bridging computer graphics and CFD. In *Proc. SIGGRAPH classes*, 25:1–25:73.

Kristof, P., Benes, B., Křivánek, J., and Stava, O. 2009. Hydraulic erosion using smoothed particle hydrodynamics. *Computer Graphics Forum 28*, 2, 219–228.

Lenaerts, T., and Dutré, P. 2009. Mixing fluids and granular materials. *Computer Graphics Forum 28*, 2, 213–218.

Lenaerts, T., Adams, B., and Dutré, P. 2008. Porous flow in particle-based fluid simulations. *ACM Trans. Graph. 27*, 3, 49:1–49:8.

Losasso, F., Talton, J., Kwatra, N., and Fedkiw, R. 2008. Two-way coupled SPH and particle level set fluid simulation. *IEEE Trans. Vis. & Comput. Graph. 14*, 4, 797–804.

Lucy, L. B. 1977. A numerical approach to the testing of the fission hypothesis. *Astronomical Journal 82*, 1013–1024.

MONAGHAN, J. J. 2005. Smoothed particle hydrodynamics. *Reports on Progress in Physics 68*, 1703–1759.

MÜLLER, M., CHARYPAR, D., AND GROSS, M. 2003. Particle-based fluid simulation for interactive applications. In *Proc. Symp. Comp. Anim.*, 154–159.

MÜLLER, M., SOLENTHALER, B., KEISER, R., AND GROSS, M. 2005. Particle-based fluid-fluid interaction. In *Proc. Symp. Comp. Anim.*, 237–244.

ONDERIK, J., CHLADEK, M., AND DURIKOVIC, R. 2011. SPH with small scale details and improved surface reconstruction. In *Proc. Spring Conf. Computer Graphics*.

ORTHMANN, J., AND KOLB, A. 2012. Temporal blending for adaptive SPH. *Computer Graphics Forum 31*, 8, 2436–2449.

ORTHMANN, J., KELLER, M., AND KOLB, A. 2010. Topology-caching for dynamic particle volume raycasting. In *Proc. Vision, Modeling & Visualization (VMV)*, 147–154.

OSHER, S., AND FEDKIW, R. 2002. *Level Set Methods and Dynamic Implicit Surfaces*. Springer-Verlag.

RAVEENDRAN, K., WOJTAN, C., AND TURK, G. 2011. Hybrid smoothed particle hydrodynamics. In *Proceedings of the 2011 ACM SIGGRAPH/Eurographics Symposium on Computer Animation*, SCA '11, 33–42.

ROSEN, M. J., AND KUNJAPPU, J. T. 2004. *Surfactants and Interfacial Phenomena*. John Wiley & Sons, Inc.

RUNGJIRATANANON, W., SZEGO, Z., KANAMORI, Y., AND NISHITA, T. 2008. Real-time animation of sand-water interaction. *Computer Graphics Forum 27*, 1887–1893.

SCHECHTER, H., AND BRIDSON, R. 2012. Ghost SPH for animating water. *ACM Trans. Graph. 31*, 4, 61:1–61:8.

SOLENTHALER, B., AND GROSS, M. 2011. Two-scale particle simulation. *ACM Trans. Graph. 30*, 81:1–81:8.

SOLENTHALER, B., AND PAJAROLA, R. 2008. Density contrast SPH interfaces. In *Proc. Symp. Comp. Anim.*, 211–218.

SOLENTHALER, B., AND PAJAROLA, R. 2009. Predictive-corrective incompressible SPH. *ACM Trans. Graph. 28*, 40:1–40:6.

SOLENTHALER, B., SCHLÄFLI, J., AND PAJAROLA, R. 2007. A unified particle model for fluid solid interactions: Research articles. *Comput. Animat. Virtual Worlds 18*, 1, 69–82.

SOLENTHALER, B., ZHANG, Y., AND PAJAROLA, R. 2007. Efficient refinement of dynamic point data. In *Proc. Symp. Point-Based Graphics*, 65–72.

STORA, D., AGLIATI, P.-O., CANI, M.-P., NEYRET, F., AND GASCUEL, J.-D. 1999. Animating lava flows. In *Graphics Interface*, 203–210.

VAN DER LAAN, W. J., GREEN, S., AND SAINZ, M. 2009. Screen space fluid rendering with curvature flow. In *Proc. Symp. Interactive 3D Graphics & Games*, 91–98.

YU, J., AND TURK, G. 2010. Reconstructing surfaces of particle-based fluids using anisotropic kernels. In *Proc. Symp. Comp. Anim.*, 217–225.

YU, J., WOJTAN, C., TURK, G., AND YAP, C. 2012. Explicit mesh surfaces for particle based fluids. *Computer Graphics Forum 31*, 2pt4 (May), 815–824.

ZHU, Y., AND BRIDSON, R. 2005. Animating sand as a fluid. *ACM Trans. Graph. 24*, 3, 965–972.

A Surface Delta Function

By definition the surface delta function is $\hat{\delta}(\mathbf{x}) = \delta(\phi(\mathbf{x}))\,||\nabla\phi(\mathbf{x})||$ [Osher and Fedkiw 2002] and $\phi(\mathbf{x}) = \min_{\mathbf{x}_s} ||\mathbf{x} - \mathbf{x}_s||$ where $\mathbf{x}_s$ is the point on the interface $\delta\Omega$ closest to $\mathbf{x}$. By assuming a flat surface $\delta\Omega = \{\mathbf{x} \in \mathbb{R}^3 | \mathbf{x} \cdot \mathbf{n} = d, |\mathbf{n}| = 1\}$ within a particle's support h we get $\nabla\phi(\mathbf{x}) = \nabla||\mathbf{x} - \mathbf{x}_s|| = d(\mathbf{x})\mathbf{n}$. By defining the closest point $\mathbf{x}_s = \mathbf{m}(\mathbf{x}) + \mathbf{n}d(\mathbf{x})$ where $d(\mathbf{x}) = \sum_j d_j V_j \hat{W}_j(\mathbf{x})$ [Adams et al. 2007] we get $\phi(\mathbf{x}) = ||\mathbf{x} - \mathbf{m}(\mathbf{x})|| - d(\mathbf{x})$. Here $d_j = \mathbf{n}^T\mathbf{x}_j$ is the distance from particle j to its closest point on the surface. For $||\nabla\phi(\mathbf{x})|| = 1$, $\mathbf{x}_s$ must be constant for all points $\mathbf{y} = \mathbf{x} + \mu\mathbf{n},\ \mu \in [0, d(\mathbf{x})]$. Hence, we have to proof that $\mathbf{m}(\mathbf{x}) + \mathbf{n}d(\mathbf{x}) = \mathbf{m}(\mathbf{y}) + \mathbf{n}d(\mathbf{y})$ which by rewriting gives $\mathbf{m}(\mathbf{x}) - \mathbf{m}(\mathbf{y}) = \mathbf{n}(d(\mathbf{x}) - d(\mathbf{y}))$. By definition $\mathbf{n}(d(\mathbf{x}) - d(\mathbf{y})) = \mathbf{nn}^T[\sum_j \mathbf{x}_j V_j \hat{W}_j(\mathbf{x}) + \sum_j \mathbf{x}_j V_j \hat{W}_j(\mathbf{y})] = \mathbf{nn}^T(\mathbf{m}(\mathbf{x}) - \mathbf{m}(\mathbf{y}))$, where $\mathbf{nn}^T \in \mathbb{R}^{3x3}$. Furthermore, $\mathbf{m}(\mathbf{x}) - \mathbf{m}(\mathbf{y}) = \alpha\mathbf{n}$, due to partition of unity of the smoothing kernels and $\alpha = d(\mathbf{x}) - d(\mathbf{y})$ due to the linearity of the plane equation. Thus, in this case, $\hat{\delta}(\mathbf{x}) = \delta(\phi(\mathbf{x}))$. An approximation of function $d(\mathbf{x})$ by a constant d [Zhu and Bridson 2005]) leads to an error of $||\nabla\mathbf{m}(\mathbf{x})||$ when omitting $||\nabla\phi(\mathbf{x})||$ in Eq. (5).

B Temporal Coherent Surfaces

A non-divergent and temporal coherent particle neighbourhood, i.e. $\nabla \cdot \mathbf{u}_i = 0$ where velocities $\mathbf{u}_{ij} = \mathbf{u}_i - \mathbf{u}_j \approx \mathbf{0}$, leads to $\frac{\partial}{\partial t}W_{ij} = \mathbf{u}_{ij} \cdot \hat{\mathbf{r}}_{ij}\,\frac{\partial}{\partial r}W_{ij} \approx 0$. By applying this identity in combination with the quotient rule we get

$$\frac{\partial}{\partial t}\mathbf{m}_i = \frac{[\sum_j V_j \frac{\partial}{\partial t}(\mathbf{x}_j W_{ij})][\sum_j V_j W_{ij}] - [\sum_j V_j \frac{\partial}{\partial t} W_{ij}][\sum_j \mathbf{x}_j V_j W_{ij}]}{[\sum_j V_j W_{ij}]^2}$$

where $\frac{\partial}{\partial t}(\mathbf{x}_j W_{ij}) = \mathbf{u}_j W_{ij} + \mathbf{x}_j \frac{\partial}{\partial t} W_{ij} \approx \mathbf{u}_j W_{ij}$, which leads to

$$\frac{\partial}{\partial t}\mathbf{m}_i = \frac{[\sum_j \mathbf{u}_j V_j W_{ij}][\sum_j V_j W_{ij}]}{[\sum_j V_j W_{ij}]^2} \approx \mathbf{u}_i \frac{[\sum_j V_j W_{ij}][\sum_j V_j W_{ij}]}{[\sum_j V_j W_{ij}]^2} = \mathbf{u}_i\,.$$

for which directly follows that $\frac{\partial}{\partial t}\phi_i = \frac{\mathbf{x}_i - \mathbf{m}_i}{||\mathbf{x}_i - \mathbf{m}_i||}(\mathbf{u}_i - \frac{\partial}{\partial t}\mathbf{m}_i) = 0$. Consequently, $\frac{\partial}{\partial t}\delta_i = \frac{\partial}{\partial \phi}\delta(\phi_i)\,\frac{\partial}{\partial t}\phi_i = 0$ as long as $\nabla \cdot \mathbf{u}_i = 0$.